# Hollow Fibre Adsorption Unit for On-board Carbon Capture: The Key to Reducing Transport Emissions

Carbon Capture Science & Technology 2 (2022) 100034

Contents lists available at ScienceDirect

Carbon Capture Science & Technology

journal homepage: www.elsevier.com/locate/ccst

Full Length Article

# Hollow Fibre Adsorption Unit for On-board Carbon Capture: The Key to Reducing Transport Emissions

Collette Larkin [1], James Morrison [1], Molly Hemmings [1], Liu Guanhong [1], Guangru Zhang [2], Fermín Oliva [3], Francisco R. García–García [1,*]

[1] School of Engineering, Institute of Materials and Processes, University of Edinburgh, Robert Stevenson Road, Edinburgh EH9 3FB, UK
[2] State Key Laboratory of Materials-Orientated Engineering, College of Chemical Engineering, Nanjing Tech University, 30 Puzhu Road(S), Nanjing 211816, PR
[3] Repsol S. A., Calle Méndez Álvaro, 44, 28045 Madrid, Spain

ARTICLE INFO

*Keywords:*
Hollow fibre adsorption unit
On-board carbon capture
Transport sector emissions
Calcium oxide
Optimised sorbent-loading
Sol-gel Pechini method

ABSTRACT

Transport is amongst the most difficult sectors to decarbonise and carbon capture and storage (CCS) presents a promising solution. However, its application in vehicles is limited by the size and weight of the capture system. The hollow fibre adsorption unit (HFAU) is more compact than mature carbon capture technologies, providing a feasible route to on-board CCS. This work studies the optimization of sorbent-loading inside an HFAU via the synthesis of five HFAUs with increasing sorbent-loading per unit. The HFAUs were formed by impregnating $\alpha$-$Al_2O_3$ hollow fibre supports with CaO. The performance of the HFAUs was tested under five $CO_2$ adsorption/desorption cycles (*i.e.* adsorption at 650°C, 1 atm; desorption at 900°C, 1 atm). A feed gas with $CO_2$ concentrations mimicking vehicle exhaust streams (14 vol% $CO_2$ balanced in air) was used for adsorption. The HFAU subjected to three impregnations (*i.e.* HFAU3) achieved the highest total capacity and breakthrough capacity of 5% $CO_2$ per unit length, demonstrating that the CaO-loading can be optimised to maximise performance whilst reducing sorbent requirements, unit size and costs. The performance of HFAU3 was compared against a packed bed adsorption unit (PBAU) using an equivalent mass of CaO tested under the same reaction conditions. HFAU3 achieved a breakthrough capacity of 5% $CO_2$ per unit volume that was 3.3 times greater than that of the PBAU due to HFAU3 achieving an intensified contact between the CaO and $CO_2$. This work provides critical information to advance the design of future HFAUs and validates their potential for on-board CCS.

## 1. Introduction

The biggest contributor to global carbon dioxide ($CO_2$) emissions, aside from electricity and heat, is the transport sector (bib1, Transport, and Environment 2018). Despite improvements in vehicle efficiency, transport $CO_2$ emissions are predicted to increase further at a rate faster than other energy end-use sectors such as industrial or residential. This is due to a growing demand for global travel and faster transport modes in emerging economies (Edenhofer et al., 2014, de Blas et al., 2020, Creutzig et al., 2015). In this regard, transport is consistently recognised as one of the most challenging sectors to decarbonise, making it difficult to meet net-zero targets by 2050 (Edenhofer et al., 2014, de Blas et al., 2020).

Two well-known approaches to mitigate transport $CO_2$ emissions are: increasing the energy efficiency of the internal combustion engine or switching to a less carbon-intensive fuel such as electricity, hydrogen, ammonia or biofuels. However, neither improving engine energy efficiency nor using less carbon-intensive fuels can establish a net-zero transport sector by 2050 alone. Improvements in the energy efficiency of internal combustion engines can be achieved through optimisation of the combustion mechanism and after-treatments to increase the fuel-to-work conversion (Kalghatgi, 2019, Xin and Pinzon, 2014). However, these improvements may be superseded by a significant increase in the number of vehicles as global car ownership rates are projected to increase by 60% by 2070 (Asian Development Bank 2010, Ritchie, 2020). Switching to a less carbon-intensive fuel has received great interest, in particular, electricity with the emergence of electric vehicles powered by batteries or hydrogen fuel cells (Kalghatgi, 2018). However, the wide-scale deployment of electricity and other less carbon-intensive fuels is restrained by its developing supply chain and a lack of refuelling infrastructure (Kalghatgi, 2019). Therefore, replacing all fossil fuel-powered vehicles with less carbon-intensive fuels to meet net-zero will require substantial investment and high amounts of materials and energy at rates that may be damaging to the environment (Kalghatgi, 2018). As a result, another mitigation strategy is needed.

* Corresponding author: +44(0)131 6504860
*E-mail address:* francisco.garcia-garcia@ed.ac.uk (F.R. García–García).

https://doi.org/10.1016/j.ccst.2022.100034
Received 19 January 2022; Received in revised form 3 February 2022; Accepted 5 February 2022

An alternative approach used by power plants is to implement carbon capture and storage (CCS). Here, $CO_2$ is removed by a separation process, stored and transported to a permanent storage location (Koytsoumpa et al., 2018, Leung et al., 2014, Mertz et al., 2005). Many $CO_2$ separation processes exist, including $CO_2$ adsorption on solid sorbents and membrane separation, however, the most mature carbon capture technology uses amine-based absorption (Fan, 2015, Rochelle, 2009, Khan et al., 2011, Raynal et al., 2011). CCS has not yet been commercially applied to vehicles due to their low $CO_2$ exit concentrations, intermittent emission loads and space and weight limitations (Sharma and Maréchal, 2019). Nevertheless, because of the significant time constraint transport faces to meet net-zero 2050 targets, companies such as Repsol S.A., Mitsubishi Heavy Industries Ltd and Saudi Aramco are striving to make on-board CCS a reality (Morgan, 2020, Aramco November 11, 2020).

In the shipping industry, on-board CCS is considered to be a promising approach due to the low technology readiness level (TRL) of carbon-neutral fuel for maritime vessels and the long lifespan of current and planned petroleum-powered ships (Kalghatgi, 2019). Moreover, on-board CCS is a viable approach for shipping vessels since space and weight limitations are less constrained than other modes of transport. In 2020, Mitsubishi Heavy Industries Ltd announced the construction and trial of the world's first CCS system for shipping vessels. The trial aims to reduce shipping emissions by up to 90% by retrofitting a modified CCS system designed for onshore power plants to a coal carrier in service (Morgan, 2020). Many of the projects investigating on-board CCS for shipping vessels utilise amine-based absorption due to the maturity of the technology. However, in applications where the user is close to this type of carbon capture technology, the health issues posed by the toxicity and corrosivity of amines should be considered.

Likewise, Saudi Aramco is studying on-board CCS and in 2011, implemented a carbon capture system prototype inside a Ford F-250 pickup truck that used a solid sorbent to capture 10% of the $CO_2$ emissions (Aramco November 11, 2020). Nonetheless, carbon capture systems that use a packed bed adsorption unit with solid sorbent typically face issues such as wide residence time distributions with multiple peaks, lower mass transfer rates and large pressure drops that reduce the $CO_2$ capture performance of the carbon capture system (Fogler, 2016).

Thus, for on-board CCS to be applied to any vehicle, a compact technology that does not involve toxic substances, possesses a high capture performance and can capture low $CO_2$ exit concentrations is required. A compact technology that can improve process performance could be the hollow fibre, a porous support consisting of hundreds of open, conically-shaped micro-channels perpendicularly distributed around an empty channel. This distinctive morphology gives the hollow fibre high surface-area-to-volume ratios (>3000 $m^2$ $m^{-3}$), without compromising pressure drops (García-García et al., 2012, Tai and Material, 2013). García-García et al. (García-García et al., 2012) has demonstrated that hollow fibres can be used as a support for catalysts. Moreover, when placed inside the hollow fibre, the contact between the catalyst and reactant is intensified due to external and internal diffusion limitations being minimised. Moreover, hollow fibres can exhibit narrower residence time distributions than packed bed units, resulting in greater conversion and effective contacting. This is due to the empty channel of the hollow fibre overcoming problematic flow patterns such as fluid channelling, fluid recirculation and stagnant regions which are regularly observed in packed bed units (Fogler, 2016).

For the application of a carbon capture system in a vehicle, the micro-channels of the hollow fibre support can be impregnated with a $CO_2$ sorbent to form a hollow fibre adsorption unit (HFAU). We hypothesise that an HFAU will achieve a higher $CO_2$-loading per unit of sorbent than a packed bed adsorption unit (PBAU) and will exhibit a longer lifetime. Moreover, we anticipate that the HFAU will occupy a lower volume than the PBAU to provide greater design flexibility such that it can be implemented in a vehicle, overcoming size limitations to progress on-board CCS technology.

This work aims to compare the performance of an HFAU against a PBAU and assess the feasibility of implementing each unit in a vehicle (a feed composition of 14 vol% $CO_2$ in air was selected to mimic the typical concentration of $CO_2$ present in a vehicle exhaust stream). The HFAU was formed by impregnating an $\alpha$-$Al_2O_3$ hollow fibre with calcium oxide (CaO). CaO reversibly reacts with $CO_2$ to form calcium carbonate ($CaCO_3$) (Abanades, 2002, Kierzkowska et al., 2013, Benedetti et al., 2019). CaO was selected as it is a widely-researched sorbent material with a vast range of literature reporting on its use in carbon capture. The optimum CaO-loading inside the HFAU was investigated by comparing the $CO_2$ capture performance of five HFAUs in which the number of impregnations of CaO applied to each unit was increased incrementally. Optimisation of CaO-loading inside the hollow fibre is a key step in scaling up from TRL 2 to TRL 4.

To execute this work, the following holistic approach was adopted: (i) optimisation of the CaO-loading inside the HFAU via the synthesis of five HFAUs with increasing CaO-loadings per unit using the sol-gel method and assessment of their $CO_2$ capture performance during five $CO_2$ adsorption/desorption cycles; (ii) PBAU performance assessment during five $CO_2$ adsorption/desorption cycles against the optimised HFAU; and, (iii) feasibility study of the optimised HFAU and PBAU for carbon capture in vehicles.

## 2. Materials and methods

### 2.1. Materials

CaO was synthesised by the sol-gel Pechini method. Calcium nitrate ($Ca(NO_3)_2$), ethylene glycol ($C_2H_6O_2$) and citric acid ($C_6H_8O_7$) were used to prepare a homogeneous solution of CaO. All reagents utilised were of analytical grade and were used without further purification.

### 2.2. Preparation of adsorption units

#### 2.2.1. Preparation of hollow fibre adsorption units

Asymmetric multichannel $\alpha$-$Al_2O_3$ hollow fibre supports consisting of a finger-like region and sponge-like region shown in Figure 1A were prepared using the phase inversion technique followed by sintering at high temperatures. The detailed procedures for fabricating the supports can be found elsewhere (Shi et al., 2015). The impregnation of the 10 cm long hollow fibre support with CaO precursor was carried out following the sol-gel Pechini method. This consisted of the following three-step procedure: (i) impregnation of the hollow fibre support by pipetting the homogenous sol-gel solution; (ii) drying in a ventilated oven (SciQuip Oven-55S) at 100°C for 48 h; and, (iii) calcination under a 150 mL $min^{-1}$ airflow at 900°C for 5 h using a heat ramp of 10°C $min^{-1}$ to form solid CaO. The CaO deposition was calculated by measuring the difference in weight of the HFAU before and after calcination.

The sol-gel Pechini method was repeated such that the number of impregnations (hereby referred to as impregnation loop) applied to the five HFAUs was increased incrementally with each subsequent unit as shown in Figure 1B. The HFAUs were labelled as hollow fibre adsorption unit one (HFAU1), hollow fibre adsorption unit two (HFAU2), hollow fibre adsorption unit three (HFAU3), hollow fibre adsorption unit four (HFAU4) and hollow fibre adsorption unit five (HFAU5) following the number of CaO impregnation loops applied to each HFAU.

#### 2.2.2. Preparation of packed bed adsorption unit

CaO powder was synthesised by the sol-gel Pechini method using the same sol-gel solution utilised to impregnate the HFAUs. The three-step procedure consisted of (i) forming the precursor solution; (ii) drying the solution in a ventilated oven (SciQuip Oven-55S) at 65°C overnight; and, (iii) calcining the resulting products in a static furnace (SNOL 3/1100) LHM01) under an air atmosphere at 900°C for 5 h using a heat ramp of 10°C $min^{-1}$ to form solid CaO. The CaO was pelletised by applying a load of 10 t in a 13 mm diameter cylinder for 5 min using a hydraulic

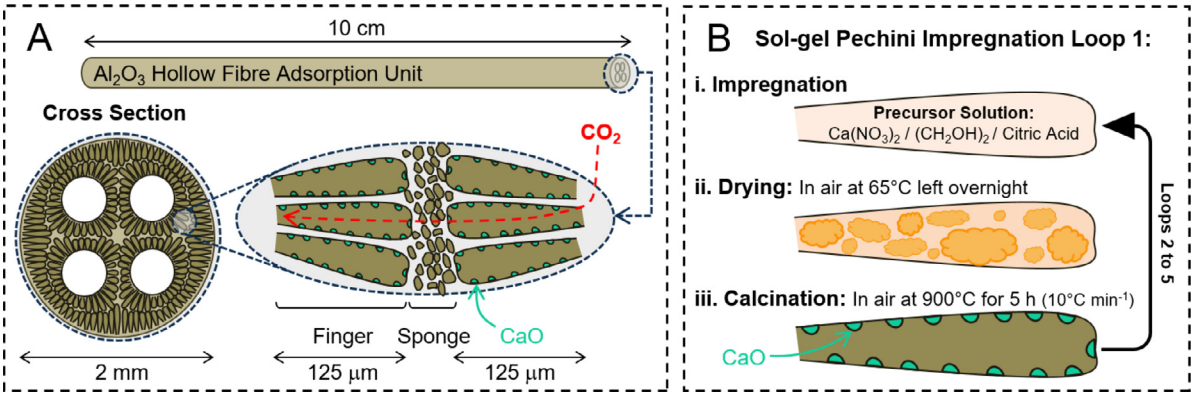


**Figure 1.** A) Hollow fibre adsorption unit made up of hundreds of radially distributed micro-channels. B) Hollow fibre impregnation loop via sol-gel Pechini method.

press (AtlasTM Manual 15T Hydraulic Press). The CaO pellets were then crushed and sieved to the p.d. of 150 $\mu$m using a stainless-steel sieve (Fieldmaster 78-800).

### 2.3. Characterisation of hollow fibre adsorption units

#### 2.3.1. Mercury intrusion porosimetry

The pore size distribution of the five HFAUs after the CaO impregnation was measured using mercury intrusion porosimetry. Mercury intrusion measurements were collected under absolute pressures ranging from 0 psi to 5000 psi with (MIP, Thermal Scientific PASCL140/440 series). The HFAUs were broken into sections of 2-3 cm in length before mercury intrusion analysis.

#### 2.3.2. Scanning electron microscopy and energy-dispersive X-ray spectroscopy

The morphology of the HFAUs after CaO impregnation was determined using Scanning Electron Microscopy (SEM) (SEM, Hitachi S-4800) operated at 20 kV. The SEM system was equipped with an energy-dispersive X-ray spectroscopy (EDX) detector that was operated at 20 kV to identify the calcium composition of the HFAUs. To secure the samples of the HFAUs to the stage, conductive adhesive tape was used.

The morphology of the optimised HFAU after five $CO_2$ adsorption/desorption test cycles was determined using SEM (Jeol, Jsm-it100) operated at 20 kV. The samples were sputter-coated with gold to enhance image quality.

### 2.4. Characterisation of the CaO pellets utilised in the PBAU

#### 2.4.1. Nitrogen adsorption/desorption isotherms at -196˚C

Surface characterisation of CaO pellets utilised in the PBAU before and after five $CO_2$ adsorption/desorption test cycles was carried out using nitrogen adsorption at -196˚C. The samples were degassed under a vacuum at 150˚C for 150 min to remove water/organic vapours present on the surfaces of the samples before nitrogen adsorption/desorption measurements were taken at 196˚C (Quantachrome Autosorb IQ). BET and BJH methods were applied to calculate the specific surface area and the pore volume of the samples, respectively.

#### 2.4.2. Scanning electron microscopy

The morphology of CaO pellets utilised in the PBAU before and after five $CO_2$ adsorption/desorption test cycles was determined using SEM (Jeol, Jsm-it100) operated at 20 kV. The samples were sputter-coated with gold to enhance image quality.

### 2.5. Performance studies of the adsorption units during $CO_2$ adsorption/desorption test cycles

#### 2.5.1. Experimental apparatus

The experimental apparatus used to undertake the adsorption/desorption test cycles was equipped with: (i) an HFAU or PBAU; (ii) a furnace (Elite Thermal Systems Limited. Model No: TSV12/32/150); (iii) a network of electrical line heaters; (iv) a gas delivery system; and, (v) a mass spectrometer (EcoSys-PTM Mass Spectrometer). See Figure S.1 of the Supplementary Information for a schematic diagram of the experimental rig used to undertake the adsorption/desorption test cycles. The equipment was controlled via a computer programme written using LabVIEW systems engineering software, allowing the opening/closing of valves of the gas delivery system. The computer was also connected to the mass spectrometer to get real-time readings of the gas composition circulating in the system. The temperatures of the lines were monitored using several k-type thermocouples distributed throughout the equipment.

#### 2.5.2. Experimental procedure

The same adsorption and desorption reaction conditions were used for all adsorption unit experiments. In accordance with the literature, the adsorption tests were undertaken at 650˚C and 1 atm while the desorption tests were undertaken at 900˚C and 1 atm (Abanades, 2002, Kierzkowska et al., 2013, Benedetti et al., 2019). The adsorption of $CO_2$ was performed using a total feed gas flow rate of 100 $cm^3$ $min^{-1}$ (STP) and the following feed mixture: 14 vol% $CO_2$ balanced in air. The desorption of $CO_2$ was performed using air as a carrier gas at a flow rate of 86 $cm^3$ $min^{-1}$ (STP). The whole experiment was designed in such a way that external and internal diffusion limitations were minimised. During the adsorption step, the composition of the exit gases was monitored by in-line mass spectrometry until ten minutes after a breakthrough had surpassed. During the desorption step, the composition of the exit gases was monitored until 30 minutes after the $CO_2$ outlet concentration was observed to be zero. The adsorption/desorption test cycles were completed five times to analyse the cyclic behaviour of each adsorption unit and stabilize the adsorption breakthrough results. Total capacity, effective capacity (defined as the capacity when a breakthrough of 5% of the $CO_2$ feed concentration was observed in the outlet stream) and lost capacity (defined as the difference between the total capacity and effective capacity) were obtained for the adsorption units at each test cycle. The total adsorption capacity represents the total amount of $CO_2$ that can be theoretically adsorbed by the adsorption unit. Whereas, the effective capacity represents the amount of $CO_2$ that can be adsorbed to achieve a 95% pure $CO_2$ outlet stream. A purity of 95% was selected as studies conducted by Pera-Titus et al (Pera-Titus et al., 2009) showed that a captured $CO_2$ stream with a molar fraction of 0.95 $CO_2$ is essential to reduce liquefaction costs. To compare the performance of the

**Table 1**
Length, total mass of CaO and mass of CaO deposited per unit length inside the five hollow fibre adsorption units (HFAUs).

| Adsorption unit | Length (cm) | Total mass of CaO (mg) | Mass of CaO per unit length (mg $cm^{-1}$) |
|---|---|---|---|
| HFAU1 | 9.2 ± 0.05 | 50.69 ± 0.02 | 5.51 ± 0.06 |
| HFAU2 | 9.5 ± 0.05 | 87.71 ± 0.02 | 9.23 ± 0.10 |
| HFAU3 | 10.0 ± 0.05 | 110.69 ± 0.02 | 11.07 ± 0.10 |
| HFAU4 | 8.0 ± 0.05 | 108.61 ± 0.02 | 13.58 ± 0.17 |
| HFAU5 | 8.0 ± 0.05 | 108.67 ± 0.02 | 13.58 ± 0.17 |

five HFAUs during $CO_2$ adsorption, the total and effective capacities obtained for each HFAU was normalised using their respective lengths. To compare the performance of the optimised HFAU against the PBAU, the total and effective capacities obtained for the two adsorption units was normalised using their respective volumes. The respective volumes of the HFAU and PBAU were kept as close practicable and at the same magnitude.

*2.5.3. Computational fluid dynamics simulations*

Computational fluid dynamics (CFD) simulations were undertaken to determine the flow pattern and velocity profile that occurs within an HFAU during the adsorption of $CO_2$. The CFD simulations were completed using StarCCM+ to calculate the boundary layer thickness, $\delta$, at a range of volumetric flow rates, including the adsorption feed flow rate at 100 $cm^3$ $min^{-1}$. A plot of volumetric flow rate, Q, against mass transfer coefficient, $k_c$, was produced using equation (1) (Fogler, 2016) by dividing the diffusion coefficient of $CO_2$ in air at 650°C, (*i.e.* $D_{CO2} = 1.27 \times 10^{-4}$ $m^2$ $s^{-1}$ (Vargaftik, 1972)), with the boundary layer thickness values obtained.

$$k_c = \frac{D_{eff}}{\delta} \quad (1)$$

The CFD simulations were also used to model the flow of gas inside the fingers and channels of the HFAU at a volumetric flow rate of 100 $cm^3$ $min^{-1}$ to simulate the flow of gas during the adsorption step.

## 3. Results

### 3.1. Optimisation of CaO-loading inside the hollow fibre adsorption units

The CaO deposited within each HFAU was calculated by measuring the difference in mass of the HFAU before and after the calcination steps. Table 1 displays the length and mass of CaO deposited inside each HFAU. Figure 2 shows the mass of CaO per unit length deposited after each impregnation loop. As expected, the mass of CaO deposited increased with each impregnation loop.

Moreover, the mass of CaO deposited per impregnation loop increased from loops one to three and plateaued after loops four and five whereby the total mass of CaO deposited reached a limit of 13.6 mg $cm^{-1}$. Observations of the data also show that although sometimes the mass of CaO deposited during an impregnation loop varied among the HFAUs, it equalised to the same value in the subsequent loop. For instance, after loop one, the mass of CaO deposited for each HFAU was around 5.5 mg $cm^{-1}$, except for HFAU3 which was 2.0 mg $cm^{-1}$. However, after loop two, the amount of CaO deposited for HFAU2 through to HFAU5 equalised to around 9.2 mg $cm^{-1}$. Similarly, after loop four, the amount of CaO deposited was 13.6 mg $cm^{-1}$ for HFAU4 while for HFAU5, it was 12.2 mg $cm^{-1}$. Nevertheless, after loop five, the final amount of CaO deposited in HFAU5 was 13.6 mg $cm^{-1}$.

### 3.2. Characterisation of hollow fibre adsorption units

*3.2.1. Scanning electron microscopy and energy-dispersive X-ray spectroscopy*

SEM images and EDX surface mapping images presented in Figure 3 display the morphology and elemental composition of the HFAUs after impregnation. SEM images at x100 magnification show that the four-channel asymmetric hollow fibre exhibits a 'sandwich' structure in which a sponge-like region lies in between two finger-like regions. EDX surface mapping images at x100 magnification suggest that the CaO was homogeneously distributed throughout each of the HFAUs and that the amount of CaO deposited increased with each impregnation loop. This is particularly noticeable around the edges of the four channels as the frequency of the calcium atoms (shown in green) increases from HFAU1 to HFAU5. SEM images at x5000 magnification confirm this observation further, with the neat porous structure that is visible in HFAU1 becoming increasingly saturated with each impregnation loop. SEM images at x25, x100 and x5000 magnification of the optimised HFAU (*i.e.* HFAU3) before and after five $CO_2$ adsorption/desorption test cycles are presented in Figure S.3A of the Supplementary Information and showed almost no change in morphology.

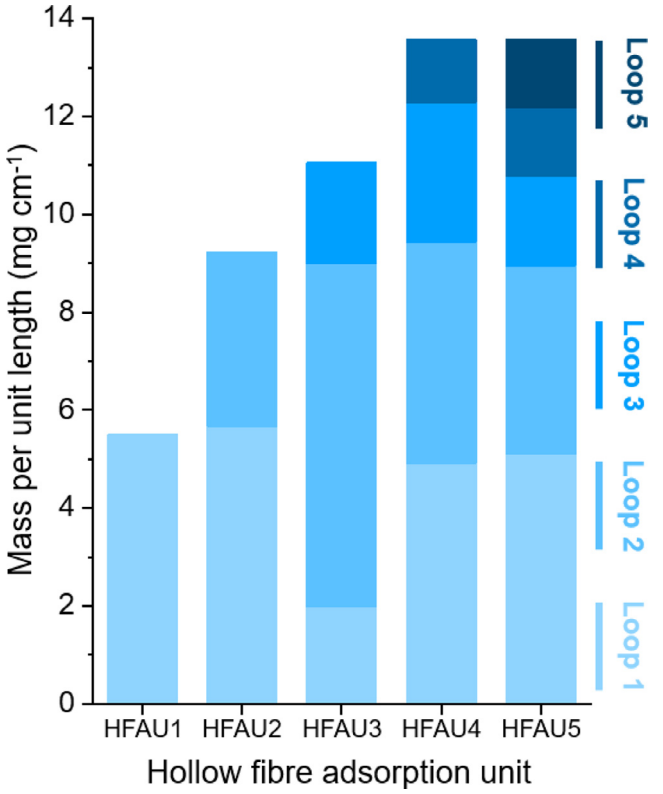


**Figure 2.** Hollow fibre adsorption units (HFAUs) versus mass per unit length of CaO deposited after each impregnation loop.

*3.2.2. Mercury intrusion porosimetry*

Deconvoluted mercury intrusion porosimetry profiles for the five HFAUs are presented in Figure 4. Two different pore size distributions can be observed for each HFAU corresponding to the entrance of the sponge-like region and the opening of the larger finger-like region. A summary of the pore size distributions obtained is reported in Table 2. For both the sponge-like and finger-like regions, the pore size distributions shifted to the left as the number of impregnation loops increased, indicating a decrease in the pore size diameter. The peak pore size diameter of the sponge-like region decreased from 0.39 $\mu$m after loop one to 0.31 $\mu$m after loop five. A similar trend was observed for the finger-like region in which the peak pore size diameter decreased from 1.68 $\mu$m after loop one to 0.74 $\mu$m after loop five. Furthermore, for both the sponge-like and finger-like regions, the intensity of the pore size distribution peaks decreased across the HFAUs as the number of impregnation loops increased.

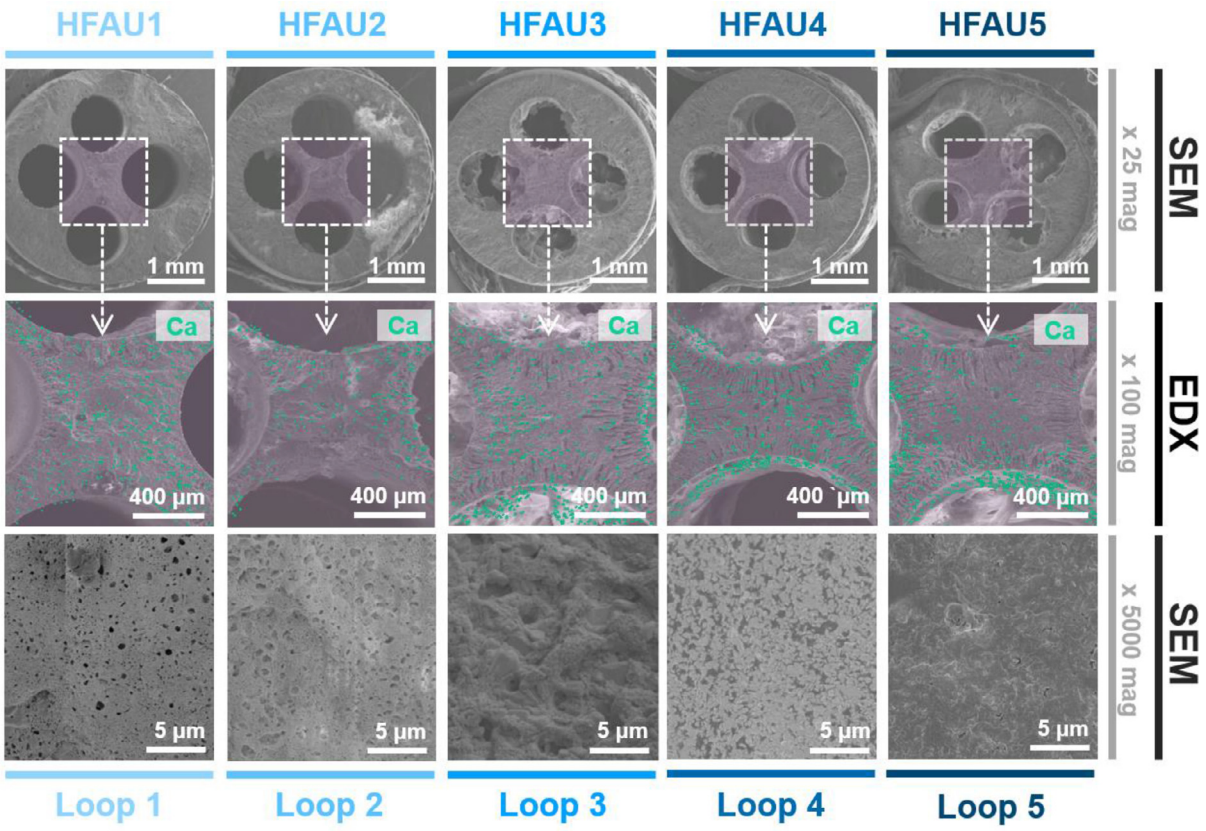


**Figure 3.** SEM images at x25, x100 and x5000 magnification of the cross-section of the hollow fibre adsorption units (HFAUs) before five $CO_2$ adsorption/desorption test cycles with the EDX elemental analysis layered over the x100 magnification SEM images.

**Table 2**
Pore size diameters of the sponge-like region and opening of the finger-like regions for the five hollow fibre adsorption units (HFAUs).

| Adsorption unit | Sponge-like region ($\mu$m) | Opening of the finger-like region ($\mu$m) |
|---|---|---|
| HFAU1 | 0.39 ± 0.01 | 1.68 ± 0.01 |
| HFAU2 | 0.39 ± 0.01 | 1.68 ± 0.01 |
| HFAU3 | 0.38 ± 0.01 | 1.53 ± 0.01 |
| HFAU4 | 0.36 ± 0.01 | 0.88 ± 0.01 |
| HFAU5 | 0.31 ± 0.01 | 0.74 ± 0.01 |

**Table 3**
Total and effective capacity per unit length of the five hollow fibre adsorption units (HFAUs) after five $CO_2$ adsorption/desorption test cycles.

| Adsorption unit | Total capacity per unit length (mg-$CO_2$ cm$^{-1}$) | Effective capacity per unit length (mg-$CO_2$ cm$^{-1}$) |
|---|---|---|
| HFAU1 | 3.8 ± 0.5 | 2.9 ± 0.4 |
| HFAU2 | 3.7 ± 0.5 | 3.1 ± 0.4 |
| HFAU3 | 7.1 ± 0.8 | 5.1 ± 0.6 |
| HFAU4 | 4.7 ± 0.6 | 3.8 ± 0.5 |
| HFAU5 | 5.7 ± 0.7 | 3.8 ± 0.5 |

### *3.3. Characterisation of the CaO pellets utilised in PBAU*

#### *3.3.1. Nitrogen adsorption/desorption isotherms at -196°C*

Nitrogen adsorption/desorption isotherms at -196°C corresponding to the CaO pellets utilised in the PBAU before and after five $CO_2$ adsorption/desorption test cycles are shown in Figure S.3B of the Supplementary Information. According to the IUPAC classification, both nitrogen adsorption/desorption isotherms are Type IV and possess a hysteresis loop Type H4, which is typical of mesoporous materials with slit-shaped pores (Sing et al., 1985). As can be seen in Figure S.3B and Table S.1 of the Supplementary Information, CaO pellets after five $CO_2$ adsorption/desorption cycles exhibit a higher surface area and pore volume (*i.e.* 98.6 m$^2$ g$^{-1}$ and 0.158 cm$^3$ g$^{-1}$, respectively) than fresh CaO pellets (*i.e.* 68.9 m$^2$ g$^{-1}$ and 0.06 cm$^3$ g$^{-1}$, respectively).

#### *3.3.2. Scanning electron microscopy*

SEM images at x100 and x5000 magnification presented in Figure S.3B showed almost no change in the morphology of the CaO pellets utilised in the PBAU before and after five $CO_2$ adsorption/desorption test cycles.

### *3.4. Performance studies of the adsorption units during five $CO_2$ adsorption/desorption test cycles*

The total, effective and lost capacity per unit length of the five HFAUs at the fifth $CO_2$ adsorption/desorption test cycle are listed in Table 3 and shown in Figure 5A. The procedure undertaken to obtain the total and effective capacity can be found in Section 3 of the Supplementary Information. The effective capacities obtained for the HFAUs at the fifth $CO_2$ adsorption/desorption test cycle were used to conduct a performance assessment comparing the optimised HFAU against a PBAU. As can be seen in Figure 5A, HFAU3 outperformed the other HFAUs in regards to their total and effective capacities per unit length (*i.e.* 5.1 mg-$CO_2$ cm$^{-1}$ and 7.1 mg-$CO_2$ cm$^{-1}$, respectively).

To conduct the performance assessment of a PBAU against the optimised HFAU, the mass of CaO used in the PBAU was made as close as practicable to that of HFAU3 (*i.e.* 112 mg for the PBAU and 111 mg for HFAU3). For HFAU3, the effective capacity per unit volume was 3.3

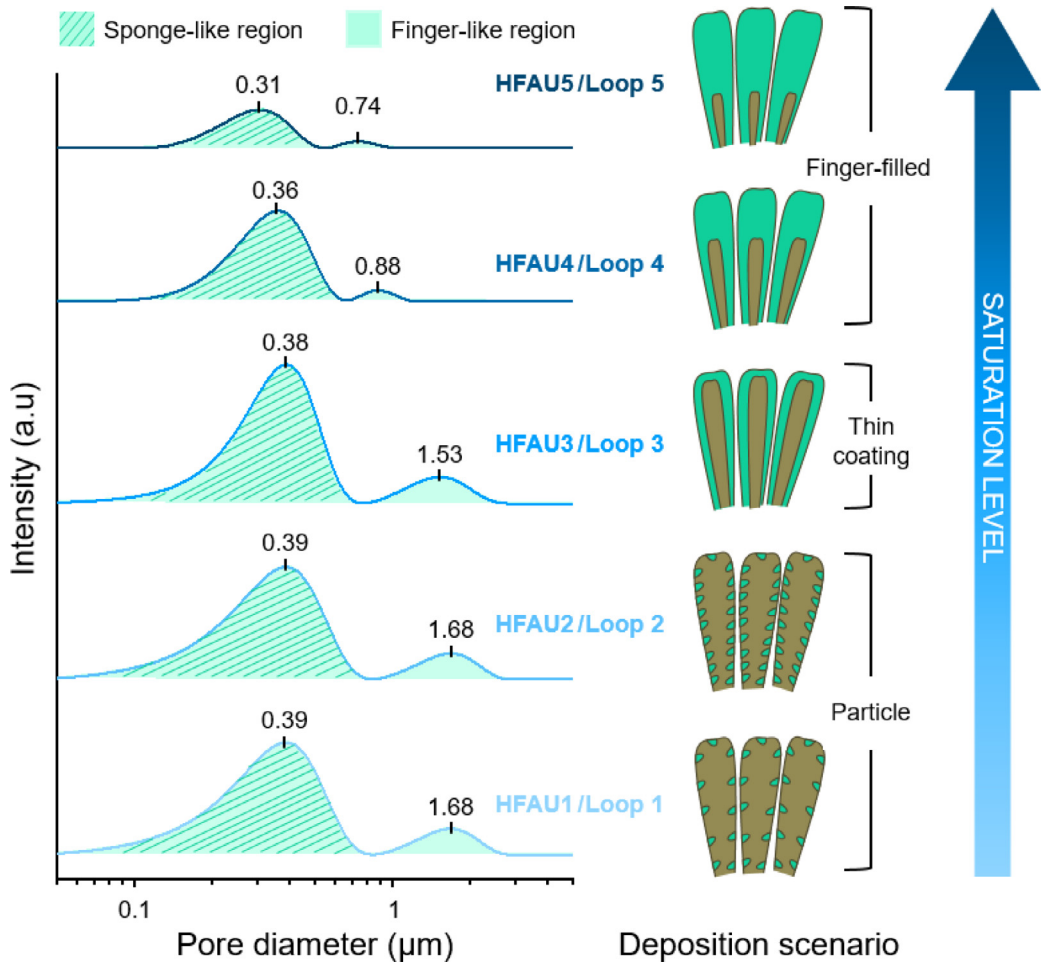


**Figure 4.** Mercury intrusion porosimetry of hollow fibre adsorption units (HFAUs)

**Table 4**
Total and effective capacity per unit volume of hollow fibre adsorption unit three (HFAU3) and the packed bed adsorption unit (PBAU) after five $CO_2$ adsorption/desorption test cycles.

| Adsorption unit | Total capacity per unit volume (mg-$CO_2$ $cm^{-3}$) | Effective capacity per unit volume (mg-$CO_2$ $cm^{-3}$) |
|---|---|---|
| HFAU3 | 227 ± 25.3 | 163 ± 18.9 |
| PBAU | 64.5 ± 7.5 | 49.8 ± 6.0 |

times greater than that of the PBAU despite the units using an equivalent total mass of CaO, see Figure 5B and Table 4.

To further understand why HFAU3 possessed a greater effective capacity per unit volume than the PBAU, the flow pattern and velocity profile inside the fingers was studied using CFD simulations. Figure 6A is an output of the data obtained by the CFD simulations and is a plot of volumetric flow rate, Q, against mass transfer coefficient, $k_c$. In Figure 6A, as the volumetric flow rate increases, the mass transfer coefficient increases until a plateau is reached at 83.3 $cm^3$ $min^{-1}$, giving an inflexion point. This divides the plot into two mass transfer limiting cases: (i) external mass transfer-limited (before inflexion point, red area); and, (ii) non-external mass transfer-limited (after inflexion point, pale blue area). Figure 6A also includes a snapshot of the simulated flow of gas inside the fingers and channel of an HFAU at 100 $cm^3$ $min^{-1}$ that shows no flow entering the fingers.

## 4. Discussion

### 4.1. Optimisation of CaO-loading inside the hollow fibre adsorption unit

The HFAU subjected to three impregnations (*i.e.* HFAU3) achieved the highest total and effective capacities per unit length at a mass of CaO per unit length of 11.1 mg $cm^{-1}$. This demonstrates that the CaO-loading inside the HFAU could be optimised to maximise performance whilst reducing costs.

Likewise, the plateau observed in Figure 2 suggests that the mass of sorbent that can be deposited within the HFAU is limited. Since the final mass of CaO per unit length deposited in HFAU4 and HFAU5 was the same at 13.6 mg $cm^{-1}$, this can be considered as the maximum. This suggests that, after five impregnation loops, the fingers within the HFAU became saturated with CaO.

### 4.2. Characterisation of hollow fibre adsorption units

#### 4.2.1. Scanning electron microscopy and energy-dispersive X-ray spectroscopy

The progressive saturation of the HFAUs observed in Figure 3 suggests that the deposition of CaO can be separated into three different scenarios. For instance, Figure 3 shows a homogenous distribution of CaO inside the fingers of HFAU1 and HFAU2 with the pores of the structure visible and unsaturated. This suggests that the CaO had not filled the fingers of the hollow fibre support. Whereas for HFAU4 and HFAU5, it can be seen that the frequency of CaO molecules deposited

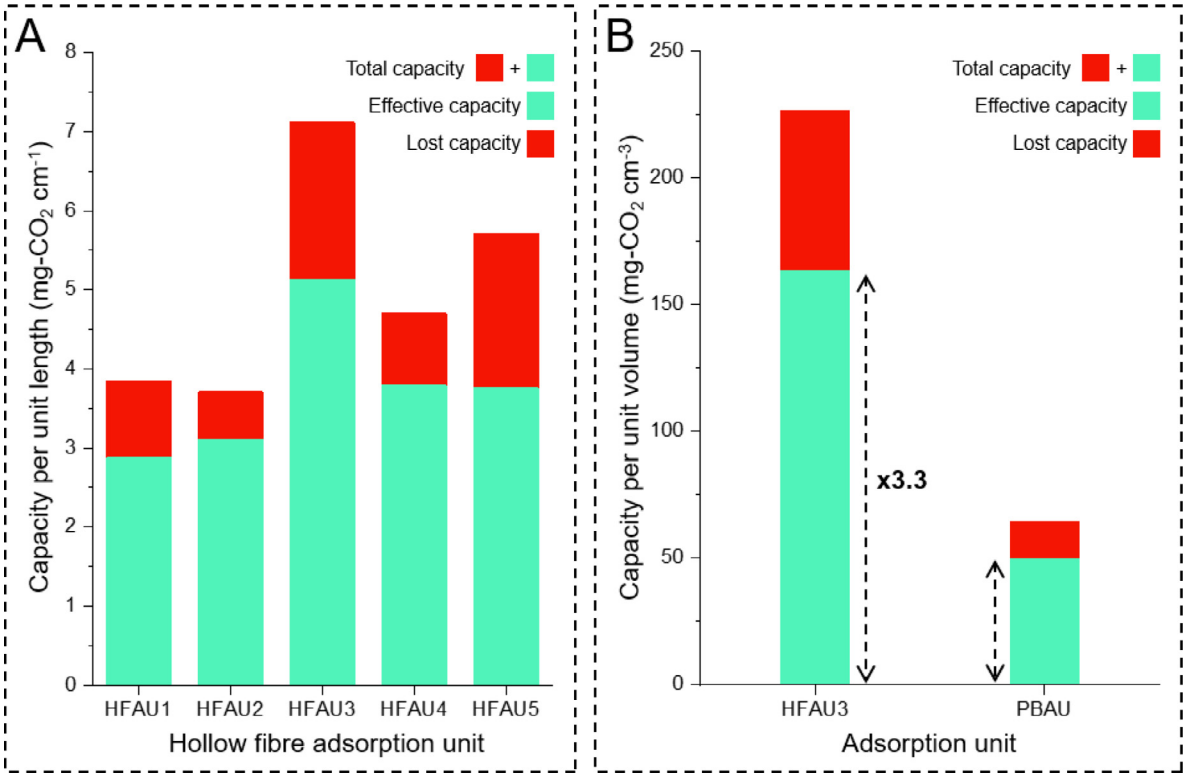


**Figure 5.** A) Performance of hollow fibre adsorption units (HFAUs) after five $CO_2$ adsorption/desorption test cycles. B) Performance of HFAU3 and the PBAU after five $CO_2$ adsorption/desorption test cycles.

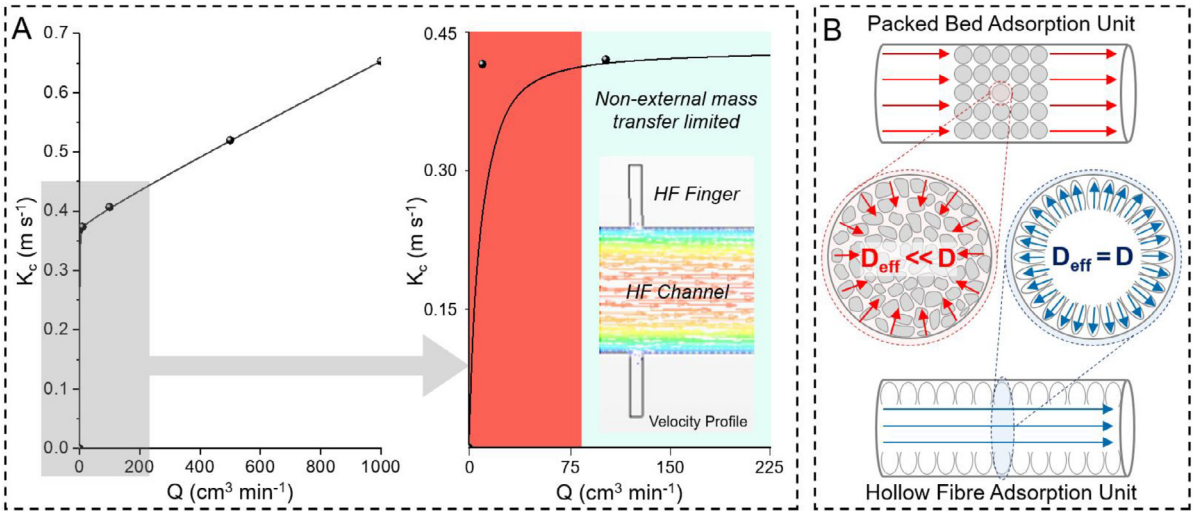


**Figure 6.** A) Volumetric flow rate against mass transfer coefficient for a hollow fibre adsorption unit (inset: computer simulation of flow rate profile inside a hollow fibre at a volume metric flow rate of 100 $cm^3\ min^{-1}$). B) Schematic showing internal diffusion inside a packed bed adsorption unit and hollow fibre adsorption unit.

had increased and the pores saturated, signifying a deposition scenario in which the CaO had filled the fingers. While for HFAU3, Figure 3 shows an increased frequency of CaO molecules with the pores visible. This suggests that in HFAU3, the CaO coated the inner surface area of the fingers without filling them.

### 4.2.2. *Mercury intrusion porosimetry*

The mercury intrusion profiles of Figure 4 agree with the SEM and EDX images of Figure 3 and provide greater insight as to what each deposition scenario looks like. The deposition scenarios have, therefore, been proposed to be: (i) particle deposition; (ii) thin coating deposition; and, (iii) finger-filled deposition and are illustrated in the schematic diagrams of Figure 4.

For HFAU1 and HFAU2, the pore size distributions of the finger-like region are identical in both peak pore size diameter (*i.e.* 1.68 $\mu$m) and intensity, suggesting that the CaO deposited did not fill the fingers nor reduced the opening to the fingers. Hence, HFAU1 and HFAU2 exhibited the particle deposition scenario which describes discrete beads of CaO covering only a portion of the inner surface area of the fingers.

For HFAU3, the pore size distributions of the finger-like region shifted to the left marginally (*i.e.* from 1.68 $\mu$m to 1.53 $\mu$m) without a decrease in intensity (the intensity of the peak is approximately equal

to that of HFAU1). This suggests that a thin layer of CaO covered the entire inner surface area of the fingers. It is important to highlight that the CaO layer was so thin it did not fill the fingers but reduced the opening of the fingers by 9 %. Therefore, HFAU3 can be described by the thin coating deposition scenario.

While, for HFAU4 and HFAU5, the pore size distributions of the finger-like regions shifted to the left considerably (*i.e.* from 1.68 $\mu$m to 0.88 $\mu$m and 0.74 $\mu$m, respectively). In addition, the intensity of the pore size distributions of the finger-like regions decreased to 87.6% and 93.9%, respectively, to that of HFAU1. The negative shift and decrease in intensity suggest that the CaO layer covering the entire inner surface area of the fingers was so thick it filled the fingers. Thus, HFAU4 and HFAU5 exhibited the finger-filled deposition scenario. The finger-filled deposition scenario builds upon the thin coating scenario. Once the inner surface area of the finger was completely coated, applying additional impregnation loops resulted in CaO depositing onto the existent CaO layer.

### 4.3. Performance studies during $CO_2$ adsorption/desorption test cycles

As shown in Figure 5A, HFAU3 possessed the highest total and effective capacity per unit length out of the five HFAUs. This behaviour can be explained by the thin coating of CaO that was deposited inside the fingers of HFAU3 which maximised the surface area offered by the $\alpha$-$Al_2O_3$ hollow fibre support, see Figure 4 (Mahyon et al., 2020). For HFAU1 and HFAU2, the deposition of CaO particles inside the fingers left surface area uncovered and not fully exploited, while for HFAU4 and HFAU5, the fingers were saturated with CaO. This reduced the surface area of CaO that was available to adsorb $CO_2$ (Grasa and Abanades, 2006, Li et al., 2012). Moreover, a thicker CaO coating in some instances may have clogged the opening of the fingers entirely. Based upon these results it seems that an optimised CaO-loading within the HFAU was achieved after impregnation loop three.

When comparing HFAU3 against the PBAU, the effective capacity per unit volume of HFAU3 was 3.3 times greater than that of the PBAU as shown in Figure 5B. This can be explained by an intensified contact achieved between the $CO_2$ and CaO due to the minimised external and internal mass transfer resistances and narrow residence time distribution offered by the morphology of the hollow fibre (García-García et al., 2012, García-Vázquez et al., 2020, Rahman et al., 2011).

For a given gas-solid reaction, it is well known that external diffusion limits the reaction at low gas velocities as the boundary layer thickness is large. Increasing the gas velocity around the pellet reduces the boundary layer thickness such that the reaction is no longer external diffusion-limited (Fogler, 2016). This phenomenon is also observed in an HFAU whereby increasing the gas velocity reduces the thickness of the boundary layer that forms as the gas flows downstream along the hollow fibre channel. The results presented in Figure 6A showed that at a volumetric flow rate of 100 $cm^3$ $min^{-1}$, the adsorption of $CO_2$ was not external diffusion-limited. This is because, after 83.3 $cm^3$ $min^{-1}$, the mass transfer coefficient had plateaued.

The internal diffusion of a gas into a pore can be described by the effective diffusion coefficient ($D_{eff}$), which is related to the bulk diffusion coefficient (D), porosity ($\varphi$), tortuosity ($\tau$), and constriction factor ($\sigma_c$), of the pore bodies inside the pellet via equation (2) (Fogler, 2016).

$$D_{eff} = \frac{D\varphi\sigma_c}{\tau} \quad (2)$$

For the pellets of a PBAU, the internal diffusion of $CO_2$ is limited by a complex network of tortuous interconnecting pathways of pore bodies with varying cross-sectional areas, giving an effective diffusion coefficient less than the bulk diffusion coefficient (Fogler, 2016). However, in an HFAU, the $CO_2$ flowed through the channel before diffusing into the micro-channels of the finger-like region. Here, the internal diffusion is governed by the opening of the fingers which possess a porosity, tortuosity and constriction factor equal to one. As can be seen in the snapshot of the simulated gas flow inside an HFAU provided in Figure 6A, the $CO_2$ only entered in the fingers via diffusion. Therefore, for an HFAU, the bulk diffusion coefficient is approximately equal to the effective diffusion coefficient. This is explained by the schematic diagram of Figure 6B which illustrates the complex pathways generated by the pore bodies of a PBAU and the straight pathways offered by the open fingers in the HFAU.

Moreover, the residence time distribution of the HFAU should be narrow due to the empty channels of a hollow fibre minimising the possibility of channelling and stagnant regions occurring during the operation of the unit. These deviations from the ideal flow pattern typically arise in packed bed systems and cause the system to be less efficient whilst also limiting its lifetime. For instance, it can be seen in Figure S.3A of the Supplementary Information that after five cycles, the thin coating of CaO inside HFAU3 showed no signs of delamination and remained on the surface of the hollow fibre support, leaving the channels empty. This suggests that after the repeated cycling of HFAU3 at elevated temperatures, the thin coating of CaO was stable. Whereas for the spent CaO pellets used in the PBAU, Table S.1 shows an increase in surface area which suggests that the CaO pellets are fracturing. This can be explained by the pellets expanding and shrinking during each adsorption/desorption cycle which causes the strength of the pellets to be weakened (Kierzkowska et al., 2013). As the pellets become more fractured, they may agglomerate to form stagnant regions that generate preferential pathways (Fogler, 2016). This would worsen the residence time distribution and lifetime of the unit. Thus, these results suggest that the HFAU exhibits a narrower residence time distribution and longer lifetime than the equivalent PBAU.

A point that deserves attention is the presence of water vapour in the exhaust gas which depending on the vehicle and fuel type, will account for approximately 11 vol% of the exhaust composition (Pera-Titus et al., 2009). There is a debate in the scientific community on the effects water has on the $CO_2$ capture performance of CaO. Water vapour may react with CaO to form $Ca(OH)_2$, which could decrease the surface area of CaO available to adsorb $CO_2$. Moreover, the presence of water vapour may further induce fragmentation of the particles, decreasing the capture efficiency of the CaO (González et al., 2016, Borgwardt, 1989). On the other hand, studies have reported that the presence of water vapour can reduce the diffusion resistance of $CO_2$ to increase $CO_2$ capture rates (Donat et al., 2012). As a result, the influence of water on the $CO_2$ capture performance of the hollow fibre-based adsorption unit will be studied in future work.

In summary, these results demonstrate that the $CO_2$ capture performance of the HFAU surpassed the traditional PBAUs used in carbon capture. To further analyse the application of carbon capture systems based on HFAU3 and the PBAU in a vehicle, a short-hand feasibility study was completed.

### 4.4. Feasibility study of adsorption units for on-board carbon capture

A short-hand feasibility study was conducted to illustrate the potential application of carbon capture systems such as the HFAU in the transport sector. One of the major constraints that limit the installation of on-board carbon capture systems is the space available in the vehicle. Therefore, this study compared 1% of the volume of two transport vessels: a light-duty vehicle (LDV) and a heavy-duty vehicle (HDV) against the volume of two carbon capture systems: one based on HFAU3 and the other based on the PBAU. A volume equal to 1% of the vehicle volume was selected as this is representative of the volume required to store captured $CO_2$ that is compressed at 73 bar on-board a gasoline-powered LDV (Sullivan and Sivak, 2012). In light of this, the volumes obtained for the carbon capture systems should be less than 140 L for the LDV and 1000 L for the HDV, respectively, in order to be readily installed onto the vehicle.

With the HFAU and PBAU-based carbon capture systems utilising CaO as the $CO_2$ capturing medium, temperature swing adsorption (TSA)

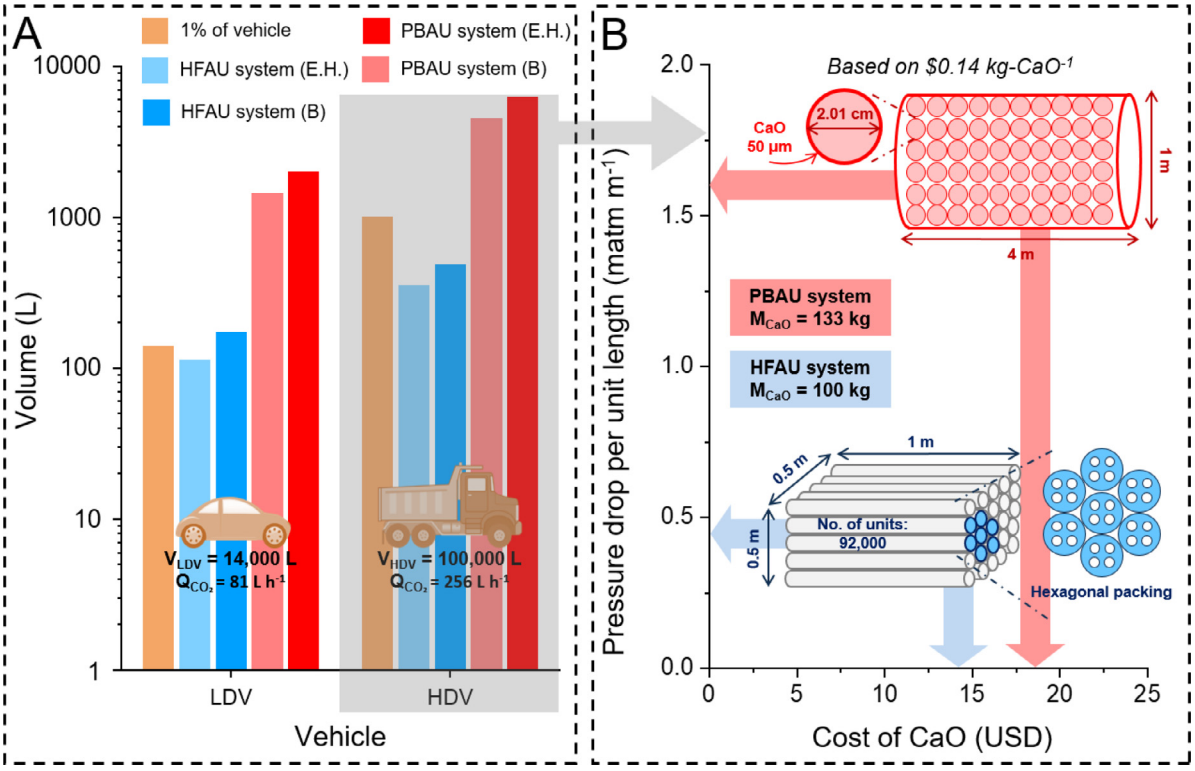


**Figure 7.** A) Volumes at 1% of the average vehicle volume for two transport vessels: light-duty vehicle (LDV) and heavy-duty vehicle (HDV) and the volumes of the HFAU-based and PBAU-based systems designed to capture the $CO_2$ emitted by each vehicle during a 100 km journey. The systems were fitted with the following heating elements: electric heater (E.H.) and burner (B). B) Cost in USD of CaO versus pressure drop per unit length for HFAU-based and PBAU-based carbon capture systems without any heating elements designed to capture the $CO_2$ emissions released by the HDV during a 100 km journey.

at atmospheric pressure was selected as the $CO_2$ separation method, see Figure S.5 of the Supplementary Information for a process flow diagram. In this TSA cycle, the exhaust gas is passed through the unit where the $CO_2$ is adsorbed by CaO and the remaining gases are released into the environment. Once the CaO is saturated with $CO_2$, it is heated to desorb the $CO_2$ and regenerate the CaO. The conditions of the exhaust gas should be taken into account when selecting which temperatures the TSA cycle should operate at. Exhaust gas temperatures of diesel engines range from 350 to 700˚C due to factors such as the engine load affecting the exhaust gas temperature significantly (Kanchibhotla and Bari, 2018). Therefore, considering a high engine load of around 100%, an adsorption temperature of 650˚C was selected (Zheng et al., 2004). This temperature is well-suited for TSA systems utilising CaO as it is thermodynamically favourable and exhibits fast kinetics (Borgwardt, 1989). For the desorption temperature, 900˚C was selected as per literature, this temperature enables reasonably fast desorption rates (Abanades, 2002, Kierzkowska et al., 2013, Benedetti et al., 2019). To complete the desorption step, an upgrade temperature of 250˚C is required. For fossil fuel-powered LDVs and HDVs, this thermal energy can be provided by burning a fraction of fuel directly under the capture unit. As a result, the volume of the capture system obtained was multiplied by 1.8 to account for the burner (ICI Caldaie 2019). Whereas for hybrid LDVs and HDVs, this thermal energy can be supplied by an electric heater which will result in an increase of volume by a factor of 1.3.

Constructing a carbon capture system based on an HFAU is straightforward due to the modularity of hollow fibres, making the scaling-up of HFAUs simple. Developing a carbon capture system based on the PBAU is more complex due to the high pressure drops associated with small particle diameters and the channelling that can take place if the ratio between the length and diameter of the unit is not optimised (Wilkins et al., 2020). The detailed procedure undertaken to conduct the feasibility study can be found in Section 4 of the Supplementary Information.

Several assumptions were considered when determining the volume of the carbon capture systems: (i) the effective capacity of the system is equal to that observed in the HFAU3 or PBAU; (ii) $CO_2$ capture recovery of 100%; (iii) adsorption takes place at 650˚C, 1 atm and desorption takes place at 900˚C, 1 atm; (iv) no heat is lost between the $CO_2$ emission source and inlet to the capture unit;(v) heating elements operate at a constant temperature and increase the volume by a factor of 1.8 and 1.3 for the burner and electric heater, respectively; and, (vi) a journey distance of 100 km. The following average direct $CO_2$ emissions per km were used to calculate the total amount of $CO_2$ released by each vehicle during a 100 km journey: (i) 150 g-$CO_2$ $km^{-1}$ for an LDV; and, (ii) 470 g-$CO_2$ $km^{-1}$ for an HDV (Edenhofer et al., 2014, Sharma and Maréchal, 2019).

The volume of the carbon capture systems required for each vehicle was determined by a series of calculations based upon the effective capacities of HFAU3 and PBAU giving the total mass of CaO required. The HFAU-based carbon capture systems consisted of thousands of hollow fibres (*i.e.* $5.9 \times 10^4$ for the LDV and $9.2 \times 10^4$ for the HDV, respectively) bundled together in a hexagonal close packing structure with a packing density of 60% (Li et al., 2004). While the PBAU-based carbon capture systems consisted of a bed of dense pellets with a diameter of 2 cm (*i.e.* $2.0 \times 10^5$ for the LDV and $6.3 \times 10^5$ for the HDV, respectively) coated with a thin layer of CaO (*i.e.* 50 $\mu$m). A bed porosity of 0.3 was then applied to account for the random packing of the dense pellets.

The results of the feasibility study are displayed in Figure 7A. The volumes calculated for the HFAU-based carbon capture system were 110 L for the LDV and 350 L for the HDV fitted with electric heaters, respectively, and 160 L for the LDV and 490 L for the HDV fitted with burners, respectively. By contrast, the volumes calculated for the PBAU-based carbon capture system were 1400 L for the LDV and 4500 L for the HDV fitted with electric heaters, respectively, and 2000 L for the LDV and 6300 L for the HDV fitted with burners, respectively. Hence, the vol-

umes obtained for the HFAU-based systems were 92% lower than those obtained for the PBAU-based systems. The smaller volumes can be attributed to the high surface-area-to-volume ratio offered by the morphology of the hollow fibre. Moreover, only the volumes of the HFAU-based systems were less than 1% of the vehicle volume for the LDV and HDV, satisfying the design criterion to enable their implementation on-board the vehicles. Although, it should be noted that for the LDV, the volume of an HFAU-based carbon capture system fitted with a burner was 10% greater than 1% of the LDV volume.

Further comparing the carbon capture systems without heating elements for the HDV, Figure 7B shows that at USD 0.14 kg-$CaO^{-1}$ (Shijiazhuang Shengping Minerals Co. Ltd 2022), the HFAU-based system is 23% cheaper than the PBAU-based system. This is due to the greater effective capacity of the HFAU lowering the amount of CaO required to capture the $CO_2$ emissions of the HDV. Furthermore, Figure 7B shows that the pressure drop per unit length obtained for the HFAU-based system was 72% lower than that of the PBAU-based system. Thus, the results of the short-hand study show that HFAU technology can overcome the space constraints, whilst reducing sorbent costs and without compromising pressure drops. Running transport vehicles with hollow fibre-based carbon capture systems, therefore, offers a feasible route towards the decarbonisation of the transport sector (Favre, 2011).

## 5. Conclusions

This work provides critical information to advance the design of future hollow fibre-based adsorption units. The thin coating of CaO inside the fingers of the HFAU achieved after three impregnation loops increased the CaO-loading without reducing the surface area available for adsorption.

The effective capacity per unit volume of the optimised HFAU (*i.e.* HFAU3) was 3.3 times greater than the PBAU despite the two units using an equal mass of CaO. The improved $CO_2$ capture performance of HFAU3 can be explained by the morphology of HFAU3 achieving an intensified contact between the $CO_2$ and CaO due to minimised mass transfer resistances and a narrow residence time distribution. After five cycles, delamination of the CaO inside HFAU3 was not observed, suggesting that the thin coating of CaO was stable on the surface of the hollow fibre support. Whereas for the spent CaO pellets of the PBAU, fracturing was observed. This indicates that the HFAU exhibits a narrower residence time distribution and longer lifetime than the equivalent PBAU.

Under real conditions, the HFAU-based carbon capture system produced a carbon capture system that was smaller (*i.e.* 92% less volume), cheaper (*i.e.* 23 wt% less CaO) and possessed a lower pressure drop (*i.e.* 72% less) than the PBAU-based carbon capture system. The overall effect was a system flexible in design that can overcome space limitations such that it can be implemented on-board a vehicle to regulate transport $CO_2$ emissions into tight emission control legislation.

The results of this work will underpin the design and development of future on-board systems that use hollow fibre technology, facilitating a cleaner transition to carbon-neutral fuel sources in the race to net-zero by 2050.

## Declaration of Comepting Interest

The authors declare that they have no known competing financial interests or personal relationships that could have appeared to influence the work reported in this paper.

The authors declare the following financial interests/personal relationships which may be considered as potential competing interests:

## Acknowledgements

C. Larkin gratefully acknowledges the funding provided by the School of Engineering at the University of Edinburgh and Repsol S.A. to carry out her PhD. The prolegomena of this work were presented as a communication at the IV UKEM Workshop in October 2020 (https://emissioncontrolukem.wordpress.com/) and as a presentation at the V UKEM Workshop in October 2021. C. Larkin would like to thank all who attended those sessions for their helpful comments and discussion.

## Supplementary materials

Supplementary material associated with this article can be found, in the online version, at doi:10.1016/j.ccst.2022.100034.

## References

Abanades, J.C., 2002. The maximum capture efficiency of CO2 using a carbonation/calcination cycle of CaO/CaCO3. Chem. Eng. J. 90, 303–306. doi:10.1016/S1385-8947(02)00126-2.

Aramco, Mobile Carbon Capture, Aramco. (n.d.). https://www.aramco.com/en/creating-value/technology-development/transport-technologies/mobile-carbon-capture# (accessed November 11, 2020).

Asian Development Bank, Reducing Carbon Emissions from Transport Projects, 2010.

Benedetti, A., Ilavsky, J., Segre, C., Strumendo, M., 2019. Analysis of textural properties of CaO-based CO2 sorbents by ex situ USAXS. Chem. Eng. J. 355, 760–776. doi:10.1016/j.cej.2018.07.164.

Borgwardt, R.H., 1989. Calcium Oxide Sintering in Atmospheres Containing Water and Carbon Dioxide. Ind. Eng. Chem. Res. 28, 493–500. doi:10.1021/ie00088a019.

Creutzig, F., Jochem, P., Edelenbosch, O.Y., Mattauch, L., van Vuuren, D.P., McCollum, D., Minx, J., 2015. Transport: A roadblock to climate change mitigation? Sci. Mag. Energy Environ. 350.

de Blas, I., Mediavilla, M., Capellán-Pérez, I., Duce, C., 2020. The limits of transport decarbonization under the current growth paradigm. Energy Strateg. Rev. 32. doi:10.1016/j.esr.2020.100543.

Donat, F., Florin, N.H., Anthony, E.J., Fennell, P.S., 2012. Influence of high-temperature steam on the reactivity of CaO sorbent for CO 2 capture. Environ. Sci. Technol. 46, 1262–1269. doi:10.1021/es202679w.

Edenhofer, O., Pichs-Madruga, R., Sokona, Y., Minx, J.C., Farahani, E., Kadner, S., Seyboth, K., Adler, A., Baum, I., Brunner, S., Eickemeier, P., Kriemann, B., Savolainen, J., Schlömer, S., von Stechow, C., Zwickel, T., IPCC, 2014: Climate Change 2014: Mitigation of Climate Change. Contribution of Working Group III to the Fifth Assessment Report of the Intergovernmental Panel on Climate Change, Cambridge, United Kingdom and New York, NY, USA, 2014. https://doi.org/10.1017/cbo9781107415416.

Fan, X., 2015. Post-Combustion Carbon Capture. Handb. Clean Energy Syst. 1–30. doi:10.1002/9781118991978.hces024.

Favre, E., 2011. Membrane processes and postcombustion carbon dioxide capture: Challenges and prospects. Chem. Eng. J. 171, 782–793. doi:10.1016/j.cej.2011.01.010.

Fogler, H.S., 2016. Elements of chemical reaction engineering, 6th ed. Prentice Hall, Philadelphia, PA.

García-García, F.R., Kingsbury, B.F.K., Rahman, M.A., Li, K., 2012. Asymmetric ceramic hollow fibres applied in heterogeneous catalytic gas phase reactions. Catal. Today. 193, 20–30. doi:10.1016/j.cattod.2012.01.006.

García-García, F.R., Torrente-Murciano, L., Chadwick, D., Li, K., 2012. Hollow fibre membrane reactors for high H 2 yields in the WGS reaction. J. Memb. Sci. doi:10.1016/j.memsci.2012.02.031.

García-Vázquez, M., Zhang, G., Hong, Z., Gu, X., García-García, F.R., 2020. Microstructured catalytic converter for residual methane emission abatement. Chem. Eng. J. 396, 125379. doi:10.1016/j.cej.2020.125379.

González, B., Liu, W., Sultan, D.S., Dennis, J.S., 2016. The effect of steam on a synthetic Ca-based sorbent for carbon capture. Chem. Eng. J. 285, 378–383. doi:10.1016/j.cej.2015.09.107.

Grasa, G.S., Abanades, J.C., 2006. CO2 capture capacity of CaO in long series of carbonation/calcination cycles. Ind. Eng. Chem. Res. 45, 8846–8851. doi:10.1021/ie0606946.

ICI Caldaie, Product catalogue, (2019). https://doi.org/10.4324/9781315771519-10.

Kalghatgi, G., 2018. Is it really the end of internal combustion engines and petroleum in transport? Appl. Energy. 225, 965–974. doi:10.1016/J.APENERGY.2018.05.076.

Kalghatgi, G., 2019. Development of Fuel/Engine Systems—The Way Forward to Sustainable Transport. Engineering 5, 510–518. doi:10.1016/j.eng.2019.01.009.

Kanchibhotla, S.A., Bari, S., 2018. Optimum Design Point to Recover Maximum Possible Exhaust Heat over the Operating Ranrticlege of a Small Diesel Truck Using Bottoming Rankine Cycle. SAE Tech. Pap. in doi:10.4271/2018-01-1377.

Khan, F.M., Krishnamoorthi, V., Mahmud, T., 2011. Modelling reactive absorption of CO2 in packed columns for post-combustion carbon capture applications. Chem. Eng. Res. Des. 89, 1600–1608. doi:10.1016/j.cherd.2010.09.020.

Kierzkowska, A.M., Pacciani, R., Müller, C.R., 2013. CaO-based CO2 sorbents: From fundamentals to the development of new, highly effective materials. ChemSusChem 6, 1130–1148. doi:10.1002/cssc.201300178.

Koytsoumpa, E.I., Bergins, C., Kakaras, E., 2018. The CO2 economy: Review of CO2 capture and reuse technologies. J. Supercrit. Fluids. 132, 3–16. doi:10.1016/j.supflu.2017.07.029.

Leung, D.Y.C., Caramanna, G., Maroto-Valer, M.M., 2014. An overview of current status of carbon dioxide capture and storage technologies. Renew. Sustain. Energy Rev. 39, 426–443. doi:10.1016/j.rser.2014.07.093.

Li, D., Wang, R., Chung, T.S., 2004. Fabrication of lab-scale hollow fiber membrane modules with high packing density. Sep. Purif. Technol. 40, 15–30. doi:10.1016/j.seppur.2003.12.019.

Li, Z., Sun, H., Cai, N., Rate Equation Theory for the Carbonation Reaction of CaO with CO 2, (2012). https://doi.org/10.1021/ef300607z.

Mahyon, N.I., Li, T., Tantra, B.D., Martinez-Botas, R., Wu, Z., Li, K., 2020. Integrating Pd-doped perovskite catalysts with ceramic hollow fibre substrate for efficient CO oxidation. J. Environ. Chem. Eng. 8, 103897. doi:10.1016/j.jece.2020.103897.

Mertz, B., Davidson, O., de Coninck, H., Loos, M., Meyer, L., IPCC, 2005. IPCC Special Report on Carbon dioxide and Storage, 2005. Prepared by Working Group III of the Intergovernmental Panel on Climate Change, Cambridge and New York.

Morgan, S., 2020. World's first 'carbon-capture at sea' set for shipping trials. EURACTIV. https://www.euractiv.com/section/energy-environment/news/worlds-first-carbon-capture-at-sea-set-for-shipping-trials/. accessed February 17, 2021.

Pera-Titus, M., Alshebani, A., Nicolas, C.H., Roumégoux, J.P., Miachon, S., Dalmon, J.A., 2009. Nanocomposite MFI-alumina membranes: High-flux hollow fibers for CO2 capture from internal combustion vehicles. Ind. Eng. Chem. Res. 48, 9215–9223. doi:10.1021/ie9004018.

Rahman, M.A., García-García, F.R., Li, K., 2011. On-board H2 generation by a catalytic hollow fibre microreactor for portable device applications. Catal. Commun. 16, 128–132. doi:10.1016/j.catcom.2011.09.016.

Raynal, L., Bouillon, P.A., Gomez, A., Broutin, P., 2011. From MEA to demixing solvents and future steps, a roadmap for lowering the cost of post-combustion carbon capture. Chem. Eng. J. 171, 742–752. doi:10.1016/j.cej.2011.01.008.

Ritchie, H., 2020. Cars, planes, trains: where do CO2 emissions from transport come from? Our World Data. https://ourworldindata.org/co2-emissions-from-transport#licence.

Rochelle, G.T., 2009. Amine Scrubbing for CO2 Capture. Science 80- (325), 1652–1654. doi:10.1126/science.1176731.

Sharma, S., Maréchal, F., 2019. Carbon Dioxide Capture From Internal Combustion Engine Exhaust Using Temperature Swing Adsorption. Front. Energy Res. 7, 1–12. doi:10.3389/fenrg.2019.00143.

Shi, Z., Zhang, Y., Cai, C., Zhang, C., Gu, X., 2015. Preparation and characterization of $\alpha$-Al2O3 hollow fiber membranes with four-channel configuration. Ceram. Int. 41, 1333–1339. doi:10.1016/j.ceramint.2014.09.065.

Shijiazhuang Shengping Minerals Co. Ltd, 2022. Factory Supply Quicklime Calcium Oxide Burnt Lime CaO Powder - Buy Quick Lime Powder, Raw Lime Powder. https://www.alibaba.com/product-detail/Factory-supply-quicklime-Calcium-Oxide-burnt_1600286563483.html?spm=a2700.7724857.normal_offer.d_title.789b5810nULHtf. accessed January 17, 2022.

Sing, K.S.., Everett, D.H., Haul, R.A.W., Moscou, L., Pierotti, R.A., Rouquerol, J., Siemieniewska, T., 1985. Reporting physisorption data for gas/solid systems with special reference to the determination of surface area an porosity (Recommendations 1984). Pure Appl. Chem. 57, 603–619. doi:10.1351/pac198557040603.

Sullivan, J.M., Sivak, M., 2012. Carbon capture in vehicles: A review of general support, available mechanisms, and consumer acceptance issues. Ann Arbor. http://deepblue.lib.umich.edu/handle/2027.42/90951.

Tai, C., Material, Y.W., Technology, I., Development of Adsorbent Hollow Fibres for Environmental Applications, (2013) 85–97. https://doi.org/10.1260/0263-6174.31.1.85.

Transport: increasing oil consumption and greenhouse gas emissions hamper EU progress towards environment and climate objectives — European Environment Agency, (n.d.). https://www.eea.europa.eu/publications/transport-increasing-oil-consumption-and/increasing-oil-consumption-and-ghg (accessed May 14, 2021).

Transport & Environment. How to decarbonise European transport by 2050., 2018. https://doi.org/10.1017/CBO9781107415324.004.

Vargaftik, N.B., Thermophysical Properties of Gases and Liquids, a Reference Book, Moscow, 1972.

Wilkins, N.S., Rajendran, A., Farooq, S., 2020. Dynamic column breakthrough experiments for measurement of adsorption equilibrium and kinetics. Adsorption 27, 397–422. doi:10.1007/s10450-020-00269-6.

Xin, Q., Pinzon, C.F., 2014. Improving the environmental performance of heavy-duty vehicles and engines: key issues and system design approaches. Altern. Fuels Adv. Veh. Technol. Improv. Environ. Perform. Towar. Zero Carbon Transp. 225–278. doi:10.1533/9780857097422.2.225.

Zheng, M., Reader, G.T., Hawley, J.G., 2004. Diesel engine exhaust gas recirculation - A review on advanced and novel concepts. Energy Convers. Manag. 45, 883–900. doi:10.1016/S0196-8904(03)00194-8.